Iodide as a Fluorescence Quencher and Promoter—Mechanisms and Possible Implications

Andriy Chmyrov, Tor Sandén, and Jerker Widengren*

Experimental Biomolecular Physics, Department of Applied Physics, Royal Institute of Technology, SE-10691 Stockholm, Sweden

Received: April 28, 2010; Revised Manuscript Received: July 1, 2010

In this work, fluorescence correlation spectroscopy (FCS) was used to investigate the effects of potassium iodide (KI) on the electronic-state population kinetics of a range of organic dyes in the visible wavelength range. Apart from a heavy atom effect promoting intersystem crossing to the triplet states in all dyes, KI was also found to enhance the triplet-state decay rate by a charge-coupled deactivation. This deactivation was only found for dyes with excitation maximum in the blue range, not for those with excitation maxima at wavelengths in the green range or longer. Consequently, under excitation conditions sufficient for triplet state formation, KI can promote the triplet state buildup of one dye and reduce it for another, red-shifted dye. This anticorrelated, spectrally separable response of two different dyes to the presence of one and the same agent may provide a useful readout for biomolecular interaction and microenvironmental monitoring studies. In contrast to the typical notion of KI as a fluorescence quencher, the FCS measurements also revealed that when added in micromolar concentrations KI can act as an antioxidant, promoting the recovery of photo-oxidized fluorophores. However, in millimolar concentrations KI also reduces intact, fluorescently viable fluorophores to a considerable extent. In aqueous solutions, for the dye Rhodamine Green, an optimal concentration of KI of approximately 5 mM can be defined at which the fluorescence signal is maximized. This concentration is not high enough to allow full triplet state quenching. Therefore, as a fluorescence enhancement agent, it is primarily the antioxidative properties of KI that play a role.

1. Introduction

Fluorescence-based spectroscopy and imaging have developed tremendously in recent years, in terms of both sensitivity and specificity, as well as with respect to spatial resolution. The photophysical and photochemical properties of the fluorescent markers provide both major bottlenecks and important prerequisites for this development. Photoswitching into transient states of fluorophores and fluorescent proteins has proven very useful for protein transport and localization studies in cells,[1] as well as to increase resolution in fluorescence-based light microscopy.[2] In addition, parameters related to the population dynamics of photoinduced, long-lived, nonfluorescent or weakly fluorescent transient states of fluorophores, generated by trans−cis isomerization, intersystem crossing, or photoinduced charge transfer, can provide additional independent information in fluorescence-based biomolecular studies.[3]

At the same time, photochemical and photophysical properties of the dyes set the limits for readout rates and sensitivity, determining the total number of photons that can be extracted per molecule (the photostability), as well as the fluorescence emission rate (the brightness). This is particularly evident in single molecule detection (SMD) or fluorescence correlation spectroscopy (FCS) applications, where a low fluorescence signal cannot be compensated by increased fluorophore concentration.

For fluorescence-based biomolecular studies, different strategies have over the years been used to improve the fluorescence emission rate and decrease photobleaching, including deoxygenation and addition of oxygen scavengers, singlet oxygen quenchers, antioxidants, or triplet state quenchers.[4−8] The basic structures of many of the dyes are to a large extent the same as those previously introduced in dye lasers, where similar strategies to improve the dye performance have been investigated and applied (see, e.g., refs 9, 10 for an overview). However, in a dye laser the conditions are relatively well defined. For biomolecular studies, large variations in environmental and experimental conditions make it more difficult to define generically useful strategies. The usefulness of a certain added compound depends on what dye it will act on and the concentration of the dye in the sample, as well as on a range of environmental factors, including viscosity, local concentrations of oxygen and of naturally occurring scavengers and quenchers, and local accessibility to the dye molecules. Also, the excitation conditions can have a substantial influence.[11−14] High excitation rates, as often used in SMD or FCS experiments, or in other applications where high readout rates or high sensitivities are required, can strongly increase the generation of several long-lived, photoinduced states of the dyes, such as triplet states, photoisomerized states, photo-oxidized states, or other states generated by photoinduced charge transfer.[8,12−15] The multitude of states generated, and the likelihood that added photostabilizers and quenchers may lead to the formation of additional intermediate states, increases the complexity. This suggests a combination of additives to be used. Along this strategy, a combination of oxygen removal and addition of both a reducing and an oxidizing agent recently proved to be useful to minimize photobleaching and blinking for a range of organic dyes.[16] In addition, for several additives there is a balance between the deactivation of triplet states and photoinduced radical states and the quenching of fluorophores in fluorescently viable states.[8] The optimal concentration of an effective additive can vary considerably depending on the combination of fluorophore/additive and the excitation conditions.

* To whom correspondence should be addressed. E-mail: jerker@biomolphysics.kth.se; phone: +46-8-55378030.

10.1021/jp103837f
Published on Web 08/09/2010

Under conditions relevant for biomolecular studies by SMD or FCS, the FCS technique itself has proven useful for characterizing population dynamics of a range of photoinduced states of dyes, including triplet states,[17] photoisomerized states,[18] and states generated by photoinduced charge transfer,[19] including photo-oxidation.[8] In this work, FCS was used to investigate the effect of potassium iodide (KI) on a set of organic dyes. Iodide is well-known to enhance intersystem crossing in organic fluorophores, in particular, by the so-called heavy atom effect.[20−22] Previously, it has been shown for several dyes that addition of KI leads to a strong enhancement of the triplet state population.[17,18] We show that for many dyes absorbing/emitting in the blue/green range addition of KI instead leads to a reduction of the triplet state population. For these dyes, an enhanced triplet state deactivation was found to take place by electron transfer between the dye and KI. Also, photo-oxidized singlet state fluorophore molecules were found to be subject to KI-mediated electron transfer. The transition rates and their KI concentration dependencies were determined, providing information about in what concentrations KI can be added, such that primarily triplet state dyes and other nonfluorescent states of the fluorophores are deactivated, rather than the fluorescently viable forms of the dyes. On the basis of this information, and when added in balanced concentrations, KI can be used as a fluorescence promoter and antifading compound. In addition, the fact that KI acts differently on different dyes and dye states suggest the role of KI as a contrast enhancement reagent for biomolecular dynamics and interaction studies.

2. Materials and Methods

The experimental setup for the FCS studies has been described before.[12,13,23,24] The fluorophore molecules under investigation were illuminated by a multiline argon-ion laser (488 nm or 514 nm, Lasos LGK 7812 ML, Jena, Germany), a helium−neon laser (594 nm, Laser2000 model 30572, Munich, Germany), or a multiline argon−krypton ion laser (568 nm or 647 nm, Melles Griot 643-RYB-A02, Carlsbad, USA), reflected by a dichroic mirror (Z488RDC, 525DCLP, Z467/568RPC, 600DCLP), and focused by a cover glass corrected water-immersion objective (Zeiss, Plan-Neofluar, 63×, 1.2 NA, 160 mm tube length) to a diameter of 0.6 μm. Single excitation wavelengths (488, 514, 568, 594, or 647 nm) were selected with excitation filters (Z488/10X, Z514/10X, Z568/10X, Z647/10X, Chroma Technology Corporation, Rockingham, USA). The fluorescent light was collected by the same objective and detected by two avalanche photodiodes (SPCM-AQR-14, Perkin-Elmer Optoelectronics, USA) in a beam splitting arrangement (50/50 nonpolarizing beam splitter cube BS010, Thorlabs, USA), to eliminate afterpulsing and dead-time effects as well as uncorrelated noise from the detectors. Typical diffusion times of the fluorophores through the detection volume were 30−40 μs at room temperature (22 ± 1 °C). Spectral filtering to remove scattered laser light was done by band-pass filters (HQ532/70M, HQ565/75M, HQ580/80M, HQ640/115M, HQ675/135M, Chroma Technology Corporation, Rockingham, USA), inserted in front of the detectors. A pinhole (30 μm diameter) was placed in the image plane to discriminate against the out-of-focus fluorescence. The signals of the two detectors were transferred to a PC-based correlator (ALV-5000 with fast option, Langen, Germany). The fluorophores used in this study (Rhodamine 6G (Rh6G), Tetramethyl Rhodamine (TMR) and ATTO488, ATTO590, ATTO610 from ATTO-TEC GmbH, Siegen, Germany, fluorescein isothiocyaniate (FITC), Rhodamine Green (RhGr), Rhodamine123 (Rh123), Alexa Fluor 488, Lissamine Rhodamine B (LRhB), Alexa Fluor 594, Alexa Fluor 610, and Alexa Fluor 633 from Invitrogen Inc., Carlsbad, USA, Cy2, Cy3, and Cy5 from GE Healthcare, Uppsala, Sweden) were dissolved from powder into DMSO and were then further diluted to nanomolar concentrations by adding ultrapure water. FITC was diluted in a 100 mM TRIS buffer (pH 8.2) to keep the fluorophore in its nonprotonated, fluorescent dianion form.

Iodobenzene (99% purity), 2-iodoethanol (99% purity), and potassium iodide (ultrapure 99.5%) were all purchased from Sigma-Aldrich (St. Louis, USA). Spectroscopically pure ethanol (99.5% purity) was purchased from Kemetyl (Haninge, Sweden).

Measurements with an expanded detection volume were performed with a similar instrumentation yielding diffusion times of 1.6 ms for the dye molecules (focal laser beam diameter, 3.2 μm; pinhole, 150 μm; objective, Olympus 60× NA 1.2; Cobolt Calypso 491 nm diode laser, Stockholm, Sweden). The measured correlation curves were fitted to the different expressions for the FCS curves as stated below, using a Levenberg−Marquardt nonlinear least-squares algorithm.

Time-correlated single photon counting (TCSPC) measurements were performed on a spectrofluorometer with a TCSPC option (FluoroMax3, Horiba Jobin Yvon, Longjumeau, France). To avoid reabsorption and re-emission effects, the fluorophore concentrations were kept strictly below 1 μM. In the TCSPC measurements, the samples were excited by a NanoLED source emitting at 495 nm with a repetition rate of 1 MHz and pulse duration of 1.4 ns. Typically, 10 000 photon counts were collected in the maximum channel using 2048 channels. The decay parameters were determined by least-squares deconvolution using a monoexponential model, and their quality was judged by the reduced χ^2 values and the randomness of the weighted residuals.

3. Theory

In FCS, for a fluorescent molecule diffusing into and out of the detection volume, and at the same time undergoing transitions to and from its lowest triplet state, the time-dependent part of the correlation function can be expressed as[17]

$$G(\tau) = \frac{1}{N(1 - T_{eq})}\left(\frac{1}{1 + \tau/\tau_D}\right)\left(\frac{1}{1 + (\omega_0/\omega_z)^2\tau/\tau_D}\right)^{1/2} \times [1 - T_{eq} + T_{eq}\exp(-\tau/\tau_T)] \quad (1)$$

Here, N is the mean number of fluorescent molecules within the detection volume. ω_0 and ω_z are the distances from the center of the laser beam focus in the radial and axial directions, respectively, at which the collected fluorescence intensity has dropped by a factor of e^2 compared to its peak value. The sample volume element is determined by the spatial distribution of the laser excitation and the collection efficiency function in the confocal setup. The characteristic diffusion time for the fluorescent molecules is given via the diffusion coefficient, D, by $\tau_D = \omega_0^2/4D$. Equation 1 assumes the collected fluorescence to be Gaussian-shaped in the axial as well as radial direction, but will under our conditions also provide a good approximation for the case of a Lorentzian-shaped axial profile of the laser beam.[23] T_{eq} is the time- and space-averaged fraction of fluorophores within the detection volume in their triplet states, and τ_T is the relaxation time related to the triplet state relaxation. With the simplifying assumption of a uniform excitation profile within the detection volume, the expressions for τ_T and T_{eq} are given by[17]

$$\tau_T = \left(k_T + \frac{\sigma I_{exc} k_{ISC}}{k_{10} + \sigma I_{exc}}\right)^{-1} \quad (2)$$

$$T_{eq} = \frac{\sigma I_{exc} k_{ISC}}{\sigma I_{exc}(k_{ISC} + k_T) + k_{10} k_T} \quad (3)$$

Here, k_{10} is the deactivation rate of the first excited singlet state, S_1, to the ground singlet state, S_0. k_{ISC} denotes the rate of intersystem crossing from S_1 to the lowest triplet state, T_1. k_T is the rate of triplet state deactivation to S_0, σ is the excitation cross section of S_0 to S_1, and I_{exc} signifies the average excitation irradiance within the detection volume.

Effects of termination of fluorescence emission of dye molecules during their passage through the volume element due to photoionization have been shown to result in an additional factor in the correlation function of eq 1[8]

$$G_R(\tau) = G(\tau)\left[1 + \frac{\dot{R}^+}{1 - \dot{R}^+} \exp(-\tau/\tau_{\dot{R}^+})\right] \quad (4)$$

where $\dot{R}^+$ is the time- and space-averaged fraction of the fluorophores in the detection volume in a photo-oxidized radical state, and $\tau_{\dot{R}^+}$ is the relaxation time of photo-oxidation/reduction.

Following photoionization of a fluorophore, its fluorescence can be recovered by collisional encounter with an antioxidant and subsequent electron transfer (Figure 1A). Due to the relatively high irradiances that can be used in FCS experiments, effects of excitation to higher singlet and triplet states (S_n and T_n states) can sometimes be noticed. In particular, from these states, photo-oxidation and photobleaching are typically strongly enhanced.[7,11−13] To describe the generation of photo-oxidized states in the FCS experiments, it is therefore beneficial to include higher excited states (S_n and T_n) into the electronic state model, as outlined in Figure 1B. At low concentrations of an antioxidant, the range of oxidation/reduction relaxation times (~100 μs) is typically much slower than the triplet relaxation times (1−2 μs in air-saturated conditions). The singlet−triplet transitions are thus equilibrated on the time scale of oxidation/reduction, and the two processes could then be treated separately. On this slower time-scale, the steady-state populations of the states within the model of Figure 1B are given by[13]

$$\begin{aligned}
S_{0eq} &= \frac{k_{Tn1} k_{Sn1} k_T k_{10}}{k_{Tn1} k_T (k_{Sn1}(k_{10} + k_{01}) + k_{01} k_{S1n}) + k_{ISC} k_{Sn1} k_{01} (k_{T1n} + k_{Tn1})} \\
S_{1eq} &= \frac{k_{01}}{k_{10}} S_{0eq} \\
T_{1eq} &= \frac{k_{ISC}}{k_T} S_{1eq} \\
S_{neq} &= \frac{k_{S1n}}{k_{Sn1}} S_{1eq} \\
T_{neq} &= \frac{k_{T1n}}{k_{Tn1}} T_{1eq}
\end{aligned} \quad (5)$$

The rate coefficients are defined in Figure 1B, with the excitation rates from S_0, S_1, and T_1 given by their corresponding excitation cross sections as $k_{01} = \sigma_{01} I_{exc}$, $k_{S1n} = \sigma_{S1n} I_{exc}$, and $k_{T1n} = \sigma_{T1n} I_{exc}$, respectively. Deactivation of the higher singlet and triplet states, S_n and T_n, have been reported to occur very rapidly, with rates k_{Sn1} and k_{Tn1} of the order 5×10^{12} s^{-1}.[13]

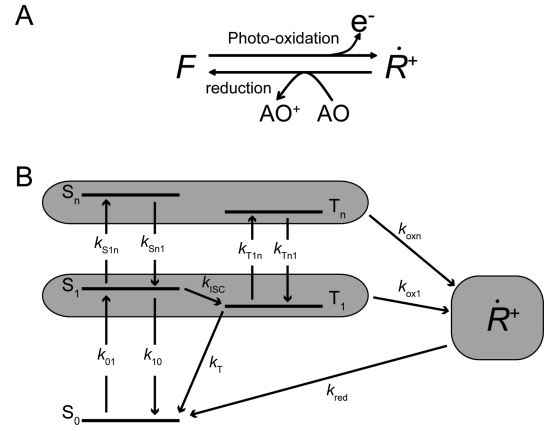

Figure 1. Major features of the photoionization/reduction process for fluorophores in the presence of an antioxidant (AO). (A) Simplified view, on a time scale at which equilibration between the singlet and triplet states has occurred (≫ triplet relaxation time, τ_T). F denotes the fluorescent, nonionized fluorophore, R^+ is the photoionized state that can be regenerated into F by donation of an electron from AO. (B) Electronic state model taking in account photoionization from both the first and the higher excited singlet (S_1 and S_n) and triplet states (T_1 and T_n). k_{ox1} and k_{oxn} denote the rate coefficients for photo-oxidation from the lower and higher excited singlet/triplet states, respectively. k_{red} is the rate of reduction by an antioxidant. k_{01} and k_{10} denote the rates of excitation from S_0 to S_1 and relaxation from S_1 to S_0 respectively. k_{ISC} and k_T are the rates of intersystem crossing from S_1 to T_1 and triplet relaxation from T_1 to S_1 respectively. k_{S1n} and k_{Sn1} are the rates of excitation from S_1 to S_n and de-excitation from S_n to S_1. k_{T1n} and k_{Tn1} are the rates of excitation from T_1 to T_n and de-excitation from T_n to T_1.

This leads to correspondingly low yields of intersystem crossing. Intersystem crossing involving S_n and T_n is therefore not included in the model of Figure 1B. From eq 5, it can be seen that the I_{exc} dependence of S_{1eq} and S_{neq} only differ by a scaling factor from that of T_{1eq} and T_{neq}, respectively. We therefore only consider the joint contribution from both T_{1eq} and S_{1eq} to the effective rate of photoionization on the one hand, and that of T_{neq} and S_{neq} on the other. In other words, we assume that the effective rate of photoionization, k_{ox}' is proportional to and takes place by equal rates, k_{ox1} and k_{oxn}, from T_{1eq}/S_{1eq} and from T_{neq}/S_{neq}, respectively. The effective rates of oxidation to $\dot{R}^+$ and reduction of $\dot{R}^+$ are then given by

$$\begin{aligned}
k_{ox}' &= k_{ox1}[S_{1eq} + T_{1eq}] + k_{oxn}[S_{neq} + T_{neq}] \\
k_{red}' &= k_{red}[AO]
\end{aligned} \quad (6)$$

Here, the effective rate of reduction of $\dot{R}^+$, denoted k_{red}', is assumed to depend on the rate of collisional interactions of $\dot{R}^+$ with an antioxidant (AO) and to be proportional to the antioxidant concentration. For fluorophores in a uniform excitation field, the relaxation time of photo-oxidation/reduction, $\tau_{\dot{R}^+}$, and the probability of finding the fluorophores in a photo-oxidized state, $\dot{R}^+$, can then be expressed as

$$\tau_{\dot{R}^+} = \frac{1}{k_{red}' + k_{ox}'} \quad (7)$$

$$\dot{R}^+ = \frac{k_{ox}'}{k_{red}' + k_{ox}'} \quad (8)$$

Under our conditions, the fluorophores within the excitation volume were assumed to be subject to an average photo-

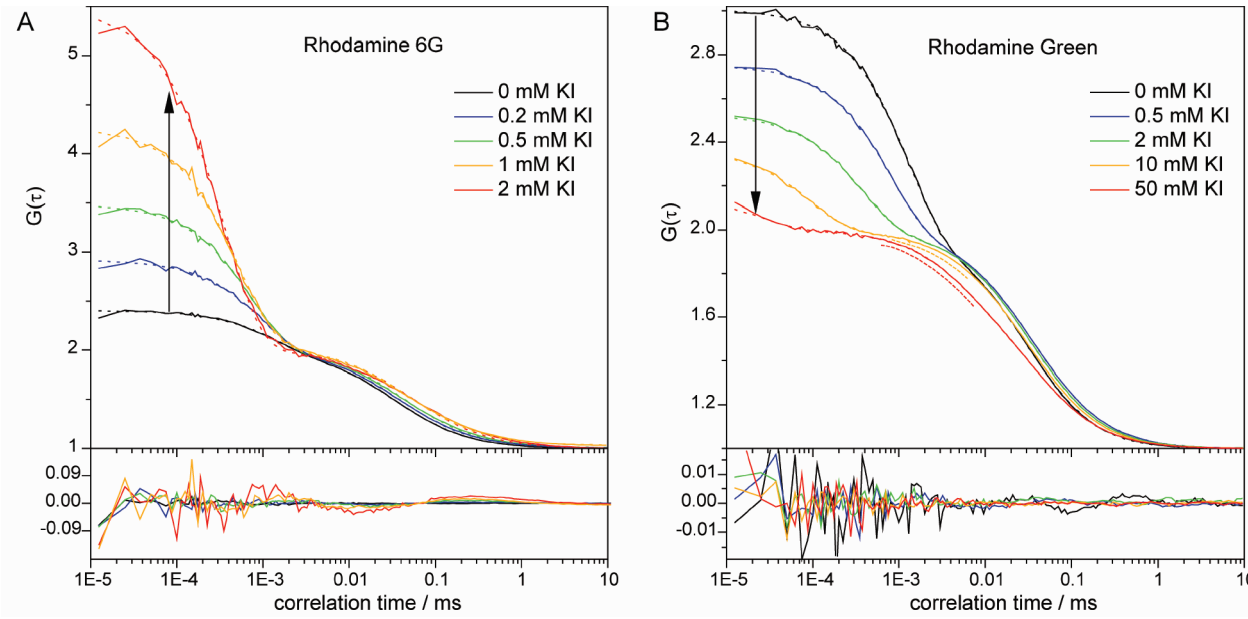

Figure 2. (A) FCS curves of Rh6G measured in aqueous solution with KI added in concentrations between 0 and 2 mM. Excitation irradiance 90 kW/cm^2. Fits and residuals obtained according to eq 1. The amplitudes of the triplet relaxation term T_{eq} and the triplet relaxation time τ_T for the different curves were determined to be 0.29/1.4 μs (0 mM), 0.48/1.0 μs (0.2 mM), 0.60/0.75 μs (0.5 mM), 0.69/0.54 μs (1 mM), and 0.78/0.35 μs (2 mM). The increase of the characteristic diffusion time τ_D, from 33 μs (0 mM) to 59 μs (2 mM), is attributed to saturation broadening of the detected fluorescence intensity profile in the presence of high triplet state populations in the detection volume. (B) FCS curves of RhGr measured in aqueous solution with KI added in concentrations between 0 and 50 mM. Excitation irradiance 350 kW/cm^2. Fits and residuals obtained according to eq 1 or eq 10: The parameters T_{eq} and τ_T were determined to be 0.50/1.3 μs (0 mM), 0.43/0.80 μs (0.5 mM), 0.35/0.37 μs (2 mM), 0.27/95 ns (10 mM), and 0.13/0.27 μs (50 mM). At the higher KI concentrations, 10 mM and 50 mM, a second relaxation process could be observed in the FCS curves (the region of the curve is indicated by an additional dashed line). The amplitude and relaxation times of this process were determined to be 0.03/4.9 μs and 0.16/4.5 μs, respectively. A minor change of τ_D from 30 μs (0 mM KI) to 33 μs (with KI) can be noted, attributed to a combination of saturation broadening and a decreased photobleaching due to a diminished triplet state buildup.

oxidation rate, k_{ox}'. However, due to the nonuniform excitation field and the different diffusion trajectories taken by the molecules through the detection volume, the fluorophores have experienced different histories of excitation. The actual space- and time-dependent magnitude of the k_{ox}' rate was shown to correspond best to an overall bimolecular reaction with a uniform relaxation rate $1/\tau_{\dot{R}^+}$ affecting a fraction of the molecules contained in the detection volume.[13] This fraction was introduced as a scaling factor of $\dot{R}^+$ and varied between 0.4 and 0.6, depending on the degree of fluorescence saturation in the experiments.

4. Results and Discussion

4.1. Selective Quenching of the Fluorophore Triplet States by KI. A range of fluorophores was investigated with respect to the effect of KI on the triplet state population dynamics. For the different dyes, KI was added in concentrations from 0.5 mM to 50 mM, and the triplet state kinetics was studied at different excitation irradiances (from 10 to 1000 kW/cm^2). From these first investigations, it was possible to identify two categories of dyes. For the first group of dyes (in order of increasing absorption wavelengths: FITC, Rh6G, TMR, LRhB, ATTO590, Alexa594, ATTO610, Alexa610, and Alexa633), a prominent increase of triplet state buildup was observed with increasing KI concentrations. This response is in good agreement with that previously observed for KI on Rh6G.[17] For the second group of fluorophores, however (in order of increasing absorption wavelengths: Alexa488, ATTO488, RhGr, and Rh123), the effect of KI was the opposite—with increasing KI concentrations, a distinct decrease of the triplet state buildup was observed. To investigate the underlying mechanisms behind the different response to KI, one dye from each category of dyes, Rh6G from the first group and RhGr from the second group, were investigated in more detail. A set of FCS curves recorded at different KI concentrations for these two dyes are shown in Figure 2. In the figure, the different responses of the two dyes can be clearly seen, with a significant increase of the triplet state population, T_{eq}, for Rh6G and a corresponding decrease of T_{eq} for RhGr. For both dyes, the triplet relaxation time τ_T was observed to significantly decrease with increasing KI concentrations. For RhGr, a second exponential relaxation process in the time range 5−10 μs could be observed in the FCS curves at KI concentrations above 5 mM (Figure 2B, dashed lines). The amplitude of this process increased with increasing KI concentrations (from 3% at 5 mM of KI to 75% at 300 mM of KI at an excitation irradiance of 800 kW/cm^2), while its relaxation time decreased (from 5 μs at 5 mM to 1 μs at 300 mM of KI, at an excitation irradiance of 800 kW/cm^2). In the FCS curves, the amplitude of this relaxation process was found to increase with higher excitation irradiances. At the same time, its relaxation time decreased, following an excitation irradiance dependence similar to that of the triplet state relaxation time. Due to the simultaneous shortening of the triplet state relaxation time upon addition of KI (generally below 300 ns at 5 mM KI and even shorter at higher KI concentrations), as well as at increasing excitation irradiances, the two relaxation times in the FCS curves could be well separated and could be analyzed and extracted by curve-fitting without significant parameter cross-covariance. The observations suggest that, except for an external heavy atom effect influencing the intersystem crossing rate from the singlet to the triplet manifold, there is at least for the second group of dyes also a triplet state deactivation mechanism present. The concomitant appearance of a second exponential process occurring in the FCS curves

of RhGr upon addition of KI indicates that the enhanced deactivation of the lowest triplet state is accompanied by a probability of transition to another, more long-lived nonfluorescent state. As a possible deactivation mechanism of the triplet state of RhGr in the presence of KI, a charge transfer-coupled reaction could be considered. This concurs well with the spectral division between the two groups of dyes. In the first group, the absorption maxima of all the dyes except FITC lie at 525 nm and above, while in the second group, all the dyes have absorption maxima below 505 nm. A possible reason why FITC does not follow the spectral division of the other fluorophores is that it is present as a dianion. Its double negative charge will to a large extent repel the I^- ions and make charge transfer between FITC and I^- less likely. From the intercept of the absorption and the emission spectra, the energy of the S_0-S_1 transition for the first group of dyes, except for FITC, can be estimated to approximately 2.30 eV or lower, and for the second group, to 2.42 eV or above. The T_1 state is lower in energy than the S_1 state, and the energy difference between these states can vary somewhat from one dye to another. Nonetheless, this distinct spectral separation of the dyes into the two groups indicates that the T_1 state of the dyes in the second group has a higher energy than what it has in the dyes from the first group. The triplet state energies of the dyes in the second group would then lie above a threshold level, above which deactivation by an electron exchange reaction with KI is possible. In contrast, for the dyes in the first group, the energy levels of their lowest triplet states are below the threshold level, and no deactivation by a charge-coupled reaction occurs. The effect of KI on the triplet state population buildup was also tested for the cyanine dyes Cy2, Cy3, and Cy5 by performing FCS measurements at different excitation irradiances (50−500 kW/cm^2, at 488, 514, and 647 nm, respectively). The measurements confirmed what has been previously observed for many cyanine dyes, that the triplet state formation of the dyes when subject to saturating excitation intensities is relatively minor, and that it is largely out-competed by photoisomerization.[25] However, in agreement with previous observations for Cy5,[18] a minor increase in the triplet state buildup could still be observed for all dyes upon addition of KI in 10 mM concentrations or higher. Hence, an increase was also observed for Cy2, which spectrally would belong to the second group of dyes above. This may indicate that the tendency for triplet states of blue-shifted dyes to be quenched by KI is not valid for cyanine dyes, but may also be related to the fact that Cy2, just like FITC, is negatively charged.

To further investigate the underlying mechanisms of the deactivation of the RhGr triplet states by KI, and what possible additional effects KI may have on the fluorescence properties of RhGr, including effects on its photo-oxidized state, FCS measurements on RhGr were performed systematically over a broader range of KI concentrations (1 μM − 300 mM). With reference to Figure 1B, transitions between the singlet and triplet states of the fluorophores typically take place in the microsecond time range. To allow collisional encounters between an individual fluorophore and iodide ions to occur within this time range, KI concentrations in the millimolar range are required. In contrast, photo-oxidized fluorophores, $\dot{R}^+$, typically have lifetimes in the millisecond time range. Many small molecular reducing agents can therefore significantly quench $\dot{R}^+$ already at micromolar concentrations. To separately investigate the possible effects of KI on the triplet and on the photo-oxidized forms of the dyes, FCS measurements were first performed in the presence of KI concentrations in the micromolar range.

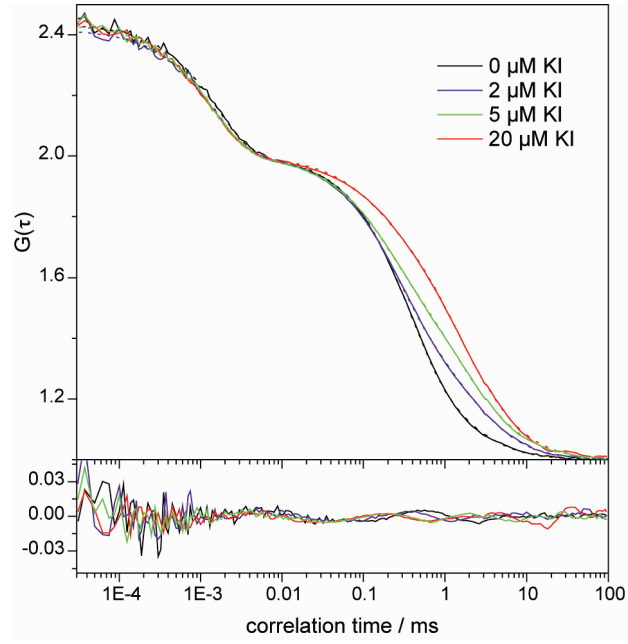

Figure 3. FCS curves of RhGr, measured in aqueous solution using an expanded detection/excitation volume at KI concentrations between 0 and 20 μM. Excitation irradiance 240 kW/cm^2. Fits and residuals performed according to eq 4. Apart from a triplet relaxation term with amplitudes/relaxation times of 0.33/1.5 μs without KI and 0.30/1.4 μs with KI present, a second relaxation process is observed with amplitudes/relaxation times of 0.42/378 μs (0 mM), 0.30/246 μs (2 μM), 0.19/159 μs (5 μM), and 0.09/117 μs (20 μM).

Thereafter, measurements were extended to KI concentrations in the millimolar range.

4.2. FCS Measurements on RhGr in the Presence of Micromolar Concentrations of KI. For KI concentrations in the micromolar range (1−50 μM), and with passage times, τ_D, of the RhGr molecules similar to those in the measurements shown in Figure 2 (~30 μs), the collisional frequency between the iodide ions, I^-, and RhGr can be expected to be too low for collisional encounters to regularly occur within the time range of τ_D. The FCS measurements in this lower KI concentration range were therefore performed with an enlarged detection volume, yielding RhGr passage times, τ_D, of 1.6 ms. With such long passage times, and with similar excitation irradiances as in Figure 2, the fluorophore molecules experience many excitation−emission cycles, which leads to an increased probability that they undergo photooxidation. This is visible in the correlation curves as a decrease in their overall decay times. In accordance with eq 4, an additional relaxation component then had to be introduced in order to fit the curves properly. With higher excitation intensities, the amplitude of this relaxation component increased, and its relaxation time decreased. Upon addition of KI in low concentrations (1−50 μM), no effect on the triplet relaxation term was observed in the FCS measurements. However, a prominent recovery of the diffusion component was visible. In contrast to the amplitude of the second relaxation process observed in the FCS curves at KI concentrations above 5 mM (Figure 2B), increasing amounts of KI decreased the radical state fraction, $\dot{R}^+$. Moreover, $\tau_{\dot{R}^+}$ was shortened, and the overall decay times of the correlation curves increased (Figure 3). With increasing KI concentrations, the additional relaxation term in the FCS curves due to photooxidation was gradually diminished and totally vanished at KI concentrations in the range 20−30 μM. This behavior is similar to that found for the well-known antioxidants *n*-propyl gallate

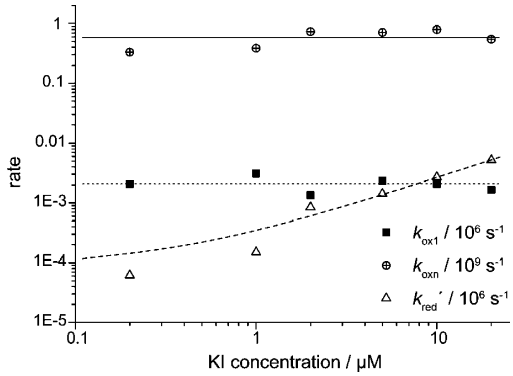

Figure 4. Rate parameters for photo-oxidation from S_1 and S_n (k_{ox1}, k_{oxn}), and for reduction from $\dot{R}^+$ (k_{red}') versus KI concentration. The rate parameters were determined by use of eqs 5−8, fitting the experimental parameters $\dot{R}^+$ and $\tau_{\dot{R}^+}$ obtained from FCS curves (eq 4), measured at different excitation irradiances and at different concentrations of KI in the micromolar range. Linear regression analysis on the k_{red}' values yields the slope $k_{red} = 2.6 \times 10^8$ M^{-1} s^{-1}. k_{ox1} and k_{oxn} show a [KI]-independent behavior with $k_{ox1} = 2.1 \times 10^3$ s^{-1} and $k_{oxn} = 5.8 \times 10^8$ s^{-1}.

(*n*PG) and ascorbic acid (AA) in a previous study.[8] Interestingly, KI is not primarily known as an antioxidant and antifading compound, as it appears to be for the dyes of the second group, but rather the opposite—as a fluorescence quencher. However, when dissociated in aqueous solution the iodide ions are known to act as mild reducing agents.[10] As an electron donor, I^- participates in a bimolecular reaction with the fluorophore molecules, which thereby return to the normal state by receiving electrons. The parameters $\dot{R}^+$ and $\tau_{\dot{R}^+}$, determined from the FCS curves, and their excitation irradiance and KI concentration dependence could be well-fitted to the kinetic scheme of Figure 1B and the eqs 5−8, according to the procedure described in ref 8. The obtained values of the oxidation and reduction rates for each concentration of KI are plotted in Figure 4. While the oxidation rates k_{ox1} and k_{oxn} remain close to constant and independent of [KI], the reduction rate, k_{red}, shows a linear dependence to [KI], from which slope a bimolecular reduction constant of photooxidized RhGr by KI of $k_{red} = 2.6 \times 10^8$ M^{-1} s^{-1} can be determined. From Figure 4, the oxidation rates k_{ox1} and k_{oxn} can be estimated as averaged values of 2.1×10^3 s^{-1} and 5.8×10^8 s^{-1}, respectively. The determined k_{ox1} and k_{oxn} rates for RhGr are in good agreement with the corresponding rates previously determined for Rh6G.[8] With regard to the uncertainty of some of the parameters used for the determination of these rates, in particular, the excitation cross sections of the higher excited singlet and triplet states, as well as the lifetimes of these states, the k_{ox1} and k_{oxn} rates can only be determined within a factor of 2 to 3. The determination of the bimolecular reduction rate constant, k_{Qred}, is less influenced by the accuracy of the parameters related to the excitation driven transitions. The k_{Qred} determined here for RhGr and KI is about an order of magnitude lower than that obtained for Rh6G and the well-known antioxidant *n*-propyl gallate (*n*PG) ($k_{Qred} = 2.3 \times 10^9$ M^{-1} s^{-1}) in our previous study.[8] The antioxidative effect of KI was also tested on Rh6G. FCS measurements of Rh6G in the presence of KI in micromolar concentrations showed that for this dye also addition of KI led to a reduction of the $\dot{R}^+$ state population and to a shortened $\tau_{\dot{R}^+}$. In contrast to the triplet states of RhGr and Rh6G, their $\dot{R}^+$ states thus show a similar behavior upon addition of KI and are both reduced by KI.

4.3. FCS Measurements on RhGr in the Presence of Millimolar Concentrations of KI. When gradually increasing the KI concentration from 0.5 mM to 50 mM, it was observed (Figure 2B) that the triplet relaxation term in the FCS curves of RhGr was diminished in amplitude and shifted to faster relaxation times (tens of nanoseconds), eventually disappearing from the time range accessible with our correlator (first time channel at 12.5 ns). At KI concentrations above 10 mM, an additional relaxation process in the time range of several microseconds could be observed (Figure 2B). Given the antioxidative effects of KI observed in micromolar concentrations, and similar to the behavior found for other antioxidants (*n*PG and ascorbic acid, AA) when applied in similar concentrations,[8] this additional relaxation process can be attributed to reduction of nonoxidized fluorophores. In analogy to eq 4, but after exchanging the photo-oxidized radial species $\dot{R}^+$ with a reduced dye radical $\dot{R}^-$, the correlation curves were analyzed according to

$$G_{\dot{R}^-}(\tau) = G(\tau)\left[1 + \frac{\dot{R}^-}{1 - \dot{R}^-}\exp(-\tau/\tau_{\dot{R}^-})\right] \qquad (9)$$

Here, $\dot{R}^-$ denotes the fraction of fluorophores in the reduced radical state and $\tau_{\dot{R}^-}$ the relaxation time for the transitions to and from this state. A modified kinetic scheme incorporating these transitions is presented in Figure 5.

The effect of KI at higher concentrations was systematically investigated by recording FCS curves at different excitation irradiancies (10 kW/cm^2 to 1 MW/cm^2), and with varying KI concentrations (in the range from 10 mM to 300 mM). The measurements were performed with a diffraction-limited observation volume, with resulting dwell times of the dye molecules in the order of 25−35 μs. At these fast passage times and in this range of KI concentrations, the fraction of photo-oxidized fluorophores, $\dot{R}^+$, is relatively low and is almost fully recovered by iodide (at 10 mM of KI the reduction rate is 2.6×10^6 s^{-1}, compared to the oxidation rate $k_{ox1} = 2.1 \times 10^3$ s^{-1}). Consequently, transitions to and from the photo-oxidized state, $\dot{R}^+$, can be disregarded in the correlation curves, and only transitions to and from the reduced radical state $\dot{R}^-$ and the triplet dynamics are considered. For these two processes, the triplet state population kinetics was found to take place on a very fast time scale (below 300 ns for 5 mM of KI and below 50 ns for 30 mM of KI), which is much shorter than that for the transitions to and from $\dot{R}^-$ (~5 μs). Due to this separation in the relaxation times, these processes can be treated independently. Consequently, to extract the kinetic rates related to singlet−triplet transitions in the presence of KI, only the states S_0, S_1, and T_1 from Figure 3A were considered and eqs 2 and 3 were used to extract the corresponding transitions rates from the measured triplet state amplitudes, T_{eq}, and relaxation times, τ_T. From TCSPC measurements, it was found that KI also promotes internal conversion from S_1 to S_0, with an overall quenching rate of S_1 by KI of 6.7×10^9 M^{-1} s^{-1}. The KI concentration dependence of the rate parameter k_{10} was also included in the triplet state kinetic analysis. The rates for KI-induced reduction of S_1 and T_1 were derived following a similar approach as was used for the analysis of the KI-induced reduction of the photo-oxidized species, $\dot{R}^+$. Due to the much faster time scale of the measured triplet state kinetics, equilibrium between the states S_0, S_1, and T_1 can be considered to have occurred on the time scale of the transitions to and from $\dot{R}^-$ (see Figure 5). Moreover, there is no evidence that the photoreduction quantum yield of the S_n and T_n states would be high enough to induce a nonlinear increase of $\dot{R}^-$ with increasing excitation irradiances, as observed for $\dot{R}^+$. Given the short lifetimes of S_n and T_n, and the resulting

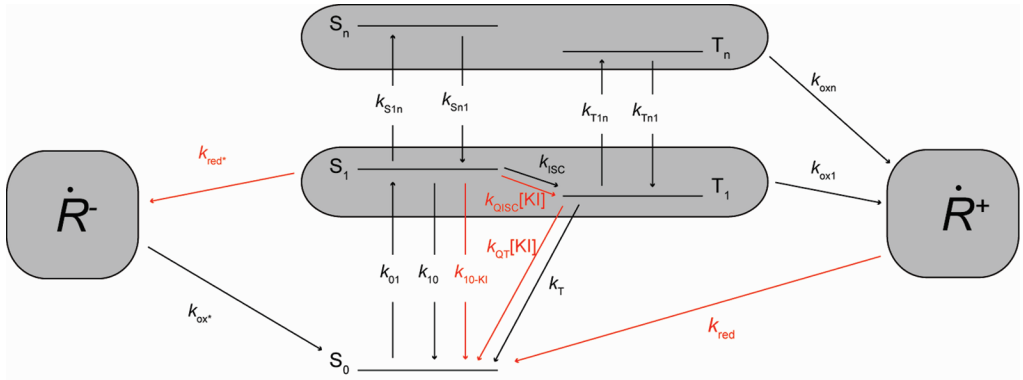

Figure 5. Kinetic scheme of photoinduced processes in RhGr, in the presence of KI at millimolar concentrations. The influence of KI on the intersystem crossing rate is denoted by the rate k_{QISC}[KI]. The triplet quenching effect of KI is denoted by the rate k_{QT}[KI]. Compared to the scheme of Figure 1B, reduction of intact viable fluorophores by iodide into the state $\dot{R}^-$ is included, together with the formation rate k_{red*}, and the KI-independent deactivation rate of this state represented by k_{ox*}. All of the KI-influenced rates are displayed in red color.

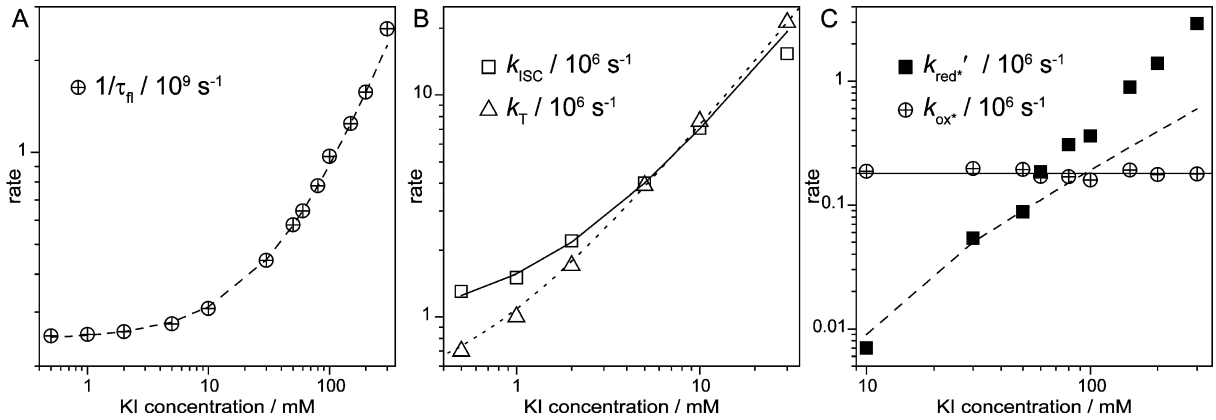

Figure 6. (A) Dependence of the fluorescence deactivation rate (the inverse of the fluorescence lifetime) on the KI concentration, as extracted from TCSPC measurements. The dashed line represents a linear fit, yielding a quenching rate of $k_{Q10} = 6.7 \times 10^9$ M^{-1} s^{-1}. (B) The [KI] dependence of k_{ISC} and k_T, as obtained from the FCS parameters T_{eq} and τ_T (eqs 2 and 3), measured at different excitation irradiances (10−800 kW/cm^2). Lines represent linear regression fits yielding the quenching rates $k_{QISC} = 0.6 \times 10^9$ M^{-1} s^{-1} and $k_{QT} = 0.7 \times 10^9$ M^{-1} s^{-1}. At 0 mM KI, $k_{ISC} = 1.0 \times 10^6$ s^{-1} and $k_T = 0.4 \times 10^6$ s^{-1}. (C) Rate parameters of iodide-induced reduction of fluorophores into $\dot{R}^-$ (k_{red*}', eq 10) and iodide-independent oxidation of $\dot{R}^-$ (k_{ox*}). k_{red*}' and k_{ox*} were obtained from the experimental parameters $\dot{R}^-$ and $\tau_{\dot{R}^-}$ by use of eqs 10 and 11. The parameters $\dot{R}^-$ and $\tau_{\dot{R}^-}$ were extracted from FCS curves, recorded at different excitation intensities at each of the indicated KI concentrations in the millimolar range, and fitted to eq 9. Lines show the outcome of linear regression analyses, yielding the slope $k_{red*} = 2.0 \times 10^6$ M^{-1} s^{-1} and $k_{ox*} = 1.8 \times 10^5$ s^{-1}. For k_{red*} and at KI concentrations higher than 50 mM, a clear deviation from a linear dependence can be observed.

low population probabilities of these states, we therefore only consider the contribution from T_1 and S_1 to the effective rate of $\dot{R}^-$ formation. Since the excitation irradiance dependencies of the populations of T_1 and S_1 only differ by a scaling factor, a joint effective reduction rate from these two states can be formulated

$$k_{red*}' = k_{red*} \times T_{eq}\left(\frac{k_T}{k_{ISC}} + 1\right) \times [KI] \qquad (10)$$

The corresponding amplitudes and relaxation times obtained by fitting the correlation curves to eq 9 are then given by

$$\dot{R}^- = k_{red*}'/(k_{ox*} + k_{red*}') \qquad (11)$$

$$\tau_{\dot{R}^-} = 1/(k_{ox*} + k_{red*}')$$

where k_{ox*} denotes the recovery rate of $\dot{R}^-$ back to S_0.

From the excitation irradiance dependence of T_{eq}, τ_T, $\dot{R}^-$, and $\tau_{\dot{R}^-}$, the rate parameters for the singlet−triplet transitions, as well as for the transitions to and from $\dot{R}^-$, could be determined for different KI concentrations by using eqs 2, 3 and 10, 11. The results of the analysis are presented in Figure 6. With increasing KI concentrations, the overall deactivation rate of S_1 ($k_{10} + k_{red*} + k_{ISC}$, or the inverse of fluorescence lifetime, τ_{fl}), the intersystem crossing rate k_{ISC} and the triplet deactivation rate k_T were all found to increase linearly with the KI concentration. In addition, for the reduction rate k_{red*} a linear increase with increasing KI concentrations was observed for KI concentrations up to 50 mM. Above that concentration, however, the k_{red*} rate starts to deviate from linearity into a more strongly increasing mode. One possible reason for such deviation is that, at these concentrations, the probability of finding a quenching molecule at any time within the quenching "sphere of action" is no longer negligible.[26] The rate of oxidation of KI-induced anions, k_{ox*}, was found to be independent of the KI concentration.

4.4. Influence on the Triplet State of RhGr by Iodobenzene and 2-Iodoethanol. From the investigations of the effects of KI on RhGr, we observe that solubilized I^- not only promotes intersystem crossing to the triplet state by an external "heavy atom" effect (i.e., an increase of the intersystem crossing rate due to an increased spin−orbital coupling in the presence of

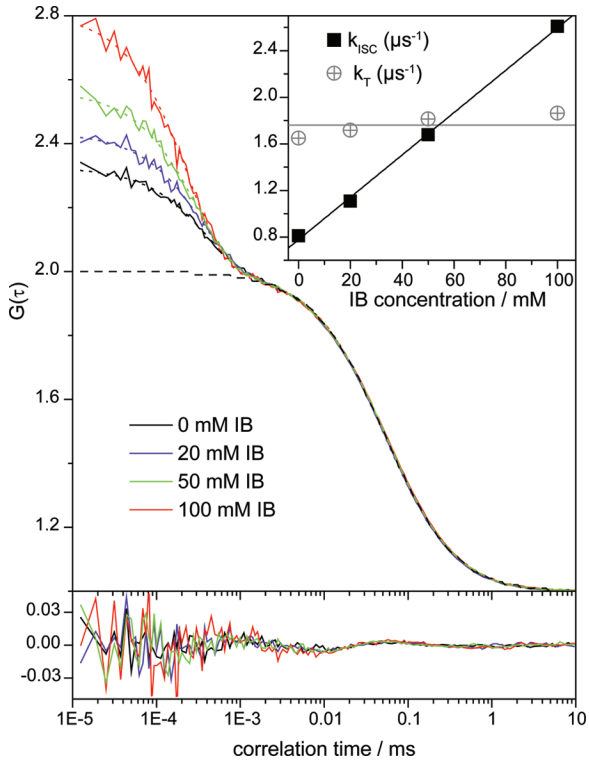

Figure 7. FCS curves of RhGr, measured in ethanol with iodobenzene (IB) in concentrations between 0 and 100 mM. Excitation irradiance = 1 MW/cm^2. Fits and residuals obtained according to eq 1. Obtained values for the amplitude of the triplet relaxation term T_{eq} and the triplet relaxation time τ_T: 0.25/401 ns (0 mM), 0.30/356 ns (20 mM), 0.36/306 ns (50 mM), 0.45/245 ns (100 mM). Diffusion time determined to τ_D = 53 μs. Inset: IB dependence of k_{ISC} and k_T on the concentration of IB, extracted from the excitation irradiance dependence (eqs 2 and 3) of the FCS parameters T_{eq} and τ_T (eq 1), measured at different excitation irradiances (50−1500 kW/cm^2). Lines represent linear regression fits yielding the quenching rate $k_{QISC} = 1.8 \times 10^7$ M^{-1} s^{-1}. k_T was found to be close to IB concentration independent, with $k_T = 1.8 \times 10^6$ s^{-1}.

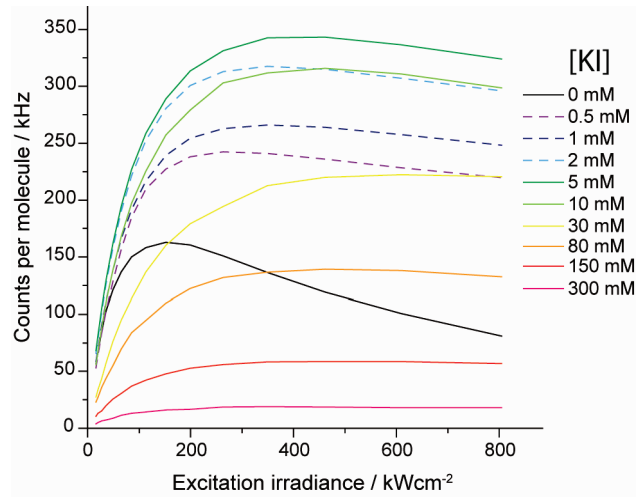

Figure 8. Counts per molecule (CPM) of RhGr without and with KI added at concentrations 0.5−300 mM, as measured by FCS versus excitation irradiances. Measurements were performed with a small excitation volume with a focal beam waist diameter of 0.6 μm. The CPM increases significantly (up to a factor of 2) with increasing [KI] up to 5 mM. At concentrations above 5 mM, effects of fluorescence quenching and KI-induced oxidation are dominating and a decrease in CPM can be noted.

an atom with high atomic number and magnetic moment), but also can deactivate the T_1 state, as well as the excited singlet states by a charge transfer reaction. In order to demonstrate and more specifically investigate the isolated "heavy atom" effect for the second group of (Rhodamine Green-like) fluorophores, measurements with iodobenzene (IB) were performed in ethanol. In these measurements, the IB concentration was varied from 0 mM up to 100 mM. For each IB concentration, the triplet state parameters τ_T and T_{eq} were extracted from the measured FCS curves (eq 1). From their excitation irradiance dependence, the rates k_{ISC} and k_T were determined using eqs 2 and 3 (with k_{10} fixed to 250 $\times$ 10^9 s^{-1} and σ set to 5 $\times$ 10^{-16} cm^2). A set of FCS curves, recorded at different IB concentrations, are shown in Figure 7, together with the determined k_T and k_{ISC} rates (inset). In contrast to KI, IB is not ionic. When IB is dissolved in ethanol, iodine is not present as an ion, but rather in a coupled form. This excludes charge transfer reactions, and dyes present in the solution are thus only expected to be influenced by a pure external heavy atom effect. Indeed, as can be seen from the FCS curves of Figure 7, there is no indication of a second relaxation process attributed to $\dot{R}^-$ formation. Rather, there is a clear increase of the triplet state fraction with increasing IB concentrations. The intersystem crossing rate was found to increase linearly with the IB concentration, while the triplet relaxation rate was found to show a very minor increase (inset of Figure 7). From the slope of the k_{ISC} versus the IB concentration, a bimolecular rate constant of $k_{QISC} = 1.8 \times 10^7$ M^{-1} s^{-1} could be determined. A similar effect as for IB in ethanol could also be observed for 2-iodoethanol in water, yielding a k_{QISC} of 2 $\times$ 10^8 M^{-1} s^{-1}. Both these bimolecular rates are more than an order of magnitude lower than that observed for KI and Rh6G in aqueous solution. In contrast to IB/2-iodoethanol and RhGr, I^- and Rh6G are oppositely charged. This, together with the larger size of 2-iodoethanol, can contribute to the lower rate constant observed for 2-iodoethanol and RhGr.

4.5. Fluorescence Brightness of RhGr at Different KI Concentrations. Given the different effects of KI on the transition rates between the electronic states of RhGr, which can influence the fluorescence yield in different and opposing directions, we investigated the effects of iodide on the fluorescence count rate per molecule (CPM, given from FCS measurements from the fluorescence intensity, divided by the parameter N in eq 1) of RhGr by adding KI at different concentrations. The outcome is shown in Figure 8. It can be seen that for KI concentrations up to 5 mM there is significant (more than 2-fold) increase in the maximum CPM. At higher KI concentrations, however, the CPM is decreasing due to a more pronounced KI-induced oxidation of intact fluorophores. This observation is in complete analogy with previous studies of the effects of mercaptoethylamine (MEA).[8] As previously found for MEA, the optimum concentration of KI is considerably lower than that required for a full triplet quenching (Figure 2B). It is rather the balance between the antioxidative properties of KI and its strength of triplet state quenching, which defines the concentration at which a maximum CPM can be reached.

4.6. Influence on Fluorophore Triplet States by Addition of TEMPO Choline. A similar, double-sided effect of both triplet state quenching and induction, as observed for KI on the dyes in the second category, can also be found for other compounds. Similar to molecular oxygen, transitions to and from the triplet state of fluorophores can also be enhanced by other paramagnetic species. Figure 9A−C shows FCS curves, monitoring the triplet state population dynamics of the dyes RhGr, Rh6G, and LRB in the presence of TEMPO choline. TEMPO

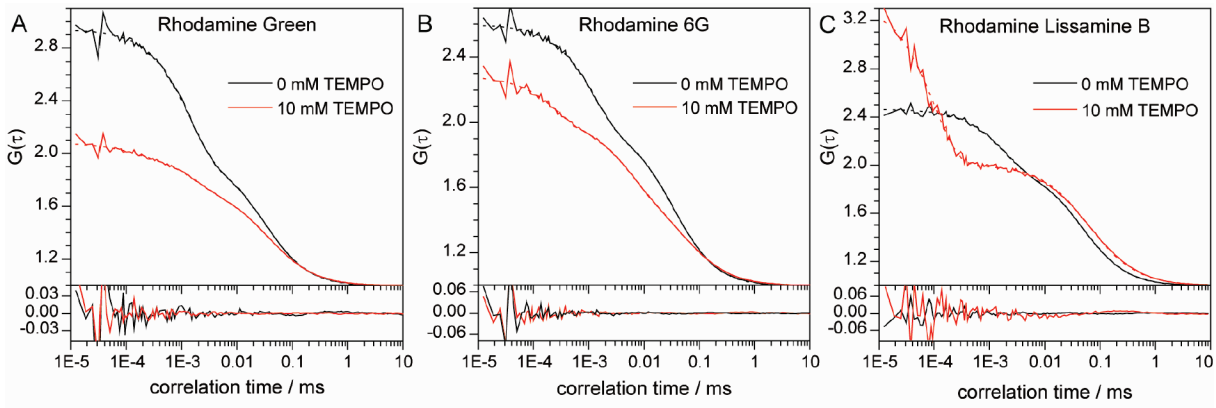

Figure 9. (A) FCS curves of RhGr measured in aqueous solution with and without TEMPO added (concentration 10 mM). Excitation irradiance 450 kW/cm^2. Fits and residuals from eq 1 and eq 9. Parameter values obtained for T_{eq} and τ_T: 0.48/1.4 μs (0 mM) and 0.07/0.12 μs (10 mM). With addition of TEMPO, a second relaxation process appeared in FCS curve, with the amplitude ($\dot{R}^-$) and relaxation time ($\tau_{\dot{R}^-}$) determined as 0.23 and 1.7 μs, respectively. (B) Corresponding experimental FCS curves, fitted curves, and residuals for Rh6G measured in aqueous solution with and without TEMPO added (concentration 10 mM). Excitation irradiance 450 kW/cm^2. T_{eq}/τ_T values of the curves: 0.37/1.2 μs (0 mM) and 0.22/0.24 μs (10 mM). In the presence of TEMPO, $\dot{R}^-$ and $\tau_{\dot{R}^-}$ were determined as 0.27 and 5.3 μs, respectively. (C) Corresponding experimental FCS curves, fitted curves, and residuals for LRB measured in aqueous solution with and without TEMPO added (concentration 10 mM). Excitation irradiance 450 kW/cm^2. T_{eq}/τ_T values of the curves: 0.32/1.7 μs (0 mM) and 0.57/0.10 μs (10 mM). For LRB, a single relaxation term in the FCS expression (eq 1) is fully sufficient to yield good fits of the experimental FCS curves.

choline is a widely used label compound in electron spin resonance spectroscopy. For certain fluorophores, such as LRB (Figure 9C), ATTO590, and Alexa594, with excitation maxima above 560 nm, a significant increase of the triplet fraction can be seen in the FCS measurements, in parallel with a decrease of the triplet state relaxation time. From the excitation irradiance dependence of τ_T and T, as obtained from the FCS curves (eq 1), and from global fits of the correlation curves (eqs 2 and 3), it can be seen that both the intersystem crossing and triplet relaxation rates increase with increasing TEMPO concentrations. Since the relative increase of k_{ISC} upon addition of TEMPO is about 3 times higher than the corresponding relative increase of k_T, the overall effect of adding TEMPO is a triplet state buildup. For the other group of fluorophores, however, with excitation maxima below 560 nm, like TMR, Rh6G (Figure 9B), and RhGr (Figure 9A), an opposite effect on the triplet state buildup can be noticed. This is analogous to the observed difference in the response to KI and its clear correlation to the spectral properties of the investigated dyes. This indicates that TEMPO also can influence the triplet states of the dyes by a similar charge-coupled enhancement of k_T. When active, this leads to a reduction of the triplet state population. On the other hand, the presence of TEMPO also seems to lead to a concomitant buildup of the reduced form of the fluorophore, similar to the results for KI.

5. Conclusions

The present investigation demonstrates that addition of KI into a dye sample can induce a manifold of effects on the population kinetics of the long-lived, photoinduced states of the dyes. Apart from a heavy atom effect promoting, in particular, intersystem crossing to the triplet state, KI can also enhance the triplet state deactivation by a charge-coupled quenching mechanism, if the energy levels of the dye triplet states are high enough. If the triplet state energy levels are sufficient for charge-coupled deactivation by KI, a KI-mediated reduction of the same dyes seems to be favored. KI is also found to act as an electron donor following photo-oxidation of these dyes, bringing the dyes back to a fluorescently viable form. A significant KI-mediated reduction of the triplet state requires KI concentrations in the mM range, while the reduction of the photo-oxidized fluorophores is already prominent at 2 orders of magnitude lower KI concentrations. Reduction of nonoxidized fluorophores in our measurements was only detectable under millimolar concentrations of KI. This mainly reflects that the lifetimes of the triplet and photoreduced states (μs) are much shorter than that of the photo-oxidized state (0.1 ms or longer). Given its triplet state quenching and antioxidative properties, KI in fact qualifies as an antifading and fluorescence enhancement compound. These beneficial properties of KI have not been brought to attention before, and are in contrast to the typical view of KI as a fluorescence quencher. One possible reason for this is that the degree of buildup of photoinduced, long-lived transient states is considerably lower under the typically much lower excitation irradiances used in conventional, ensemble fluorescence measurements. Moreover, the influence of KI and TEMPO on the triplet state parameters of fluorophores can be exploited for bimolecular interaction studies. Due to the long lifetimes of the triplet states, considerably larger relative quenching effects can be obtained than in conventional fluorescence quenching experiments, where the fluorescence lifetimes and/or the intensities are used as readout parameters.[27] The triplet population kinetics can be extracted from the fluorescence intensity fluctuations by use of FCS, as in this study, or from the time-averaged fluorescence intensity by use of modulated excitation.[3] Thereby, a strong fluorescence signal can be combined with the ability to monitor low-frequency molecular interactions, at time scales much longer than the fluorescence lifetimes. This may prove useful for, e.g., lipid−lipid, protein−lipid, and protein−protein interaction studies in biological membranes, where the collision times between the interacting molecules may well exceed the fluorescence lifetimes of the fluorophores.[28] By the use of two dyes, where accessibility of KI or TEMPO to one dye leads to triplet state buildup, and for another dye, the triplet state population is instead suppressed, an anticorrelated and spectrally separable response of the two dyes to one and the same agent can be obtained. This response can be distinguished from unspecific and accidental quenching by agents affecting the triplet states of the dyes in a similar fashion, thereby providing a higher degree of specificity and sensitivity.

Acknowledgment. This study was supported by means from EU FP7 (FLUODIAMON, 201 837), the Swedish research Council, and the Wallenberg Foundation. We authors are grateful to Prof. K.-H. Drexhage, Siegen University, and Dr. Hans Blom, KTH, Stockholm, for valuable discussions.

References and Notes

(1) Lippincott-Schwartz, J.; Altan-Bonnet, N.; Patterson, G. H. *Nat. Cell Biol.* **2003**; S7−S14.
(2) Hell, S. W. *Science* **2007**, *316*, 1153–1158.
(3) Sandeń, T.; Persson, G.; Thyberg, P.; Blom, H.; Widengren, J. *Anal. Chem.* **2007**, *79*, 3330–3341.
(4) Tsien, R. Y.; Waggoner, A. Fluorophores for Confocal Microscopy - Photophysics and Photochemistry. In *Handbook of Biological Confocal Microscopy*, 2nd ed, Pawley, J. B., Ed.; Plenum Press: New York, 1995; pp 267−280.
(5) Longin, A.; Souchier, C.; Ffrench, M.; Bryon, P. A. *J. Histochem. Cytochem.* **1993**, *41*, 1833–1840.
(6) Lichtman, J. W.; Conchello, J.-A. *Nat. Methods* **2005**, *2*, 910–919.
(7) Bernas, T.; Zarþski, M.; Dobrucki, J. W.; Cook, P. R. *J. Microsc.* **2004**, *215*, 281–296.
(8) Widengren, J.; Chmyrov, A.; Eggeling, C.; Löfdahl, P.-Å.; Seidel, C. A. M. *J. Phys. Chem. A* **2007**, *111*, 429–440.
(9) Pavlopoulos, T. G. *Prog. Quantum Electron.* **2002**, *26*, 193–224.
(10) Drexhage, K.-H. Structure and Properties of Laser Dyes. In *Dye Lasers*, 3rd ed., Schäfer, F. P., Ed.; Springer-Verlag: Berlin, 1990; pp 155−200.
(11) Benson, D. M.; Bryan, J.; Plant, A. L.; Gotto, A. M., Jr.; Smith, L. C. *J. Cell Biol.* **1985**, *100*, 1309–1323.
(12) Widengren, J.; Rigler, R. *Bioimaging* **1996**, *4*, 149–157.
(13) Eggeling, C.; Widengren, J.; Rigler, R.; Seidel, C. A. M. *Anal. Chem.* **1998**, *70*, 2651–2659.
(14) Eggeling, C.; Widengren, J.; Brand, L.; Schaffer, J.; Felekyan, S.; Seidel, C. A. M. *J. Phys. Chem. A* **2006**, *110*, 2979–2995.
(15) Zondervan, R.; Kulzer, F.; Kol'chenko, M. A.; Orrit, M. *J. Phys. Chem. A* **2004**, *108*, 1657–1665.
(16) Vogelsang, J.; Kasper, R.; Steinhauer, C.; Person, B.; Heilemann, M.; Sauer, M.; Tinnefeld, P. *Angew. Chem., Int. Ed.* **2008**, *47*, 5465–5469.
(17) Widengren, J.; Mets, Ü.; Rigler, R. *J. Phys. Chem.* **1995**, *99*, 13368–13379.
(18) Widengren, J.; Schwille, P. *J. Phys. Chem. A* **2000**, *104*, 6416–6428.
(19) Widengren, J.; Dapprich, J.; Rigler, R. *Chem. Phys.* **1997**, *216*, 417–426.
(20) Birks, J. B. *Photophysics of aromatic molecules*; John Wiley & Sons Ltd: London, 1970.
(21) Korobov, V. E.; Chibisov, A. K. *Russ. Chem. Rev.* **1983**, *52*, 27–42.
(22) Turro, N. J.; Ramamurthy, V.; Scaiano, J. C. *Principles of molecular photochemistry: an introduction*; University Science Books: Sausalito, CA, 2009.
(23) Rigler, R.; Mets, Ü.; Widengren, J.; Kask, P. *Eur. Biophys. J. Biophys.* **1993**, *22*, 169–175.
(24) Widengren, J.; Rigler, R.; Mets, Ü. *J. Fluoresc.* **1994**, *4*, 255–258.
(25) Chibisov, A. K. *J. Photochem.* **1977**, *6*, 199–214.
(26) Lakowicz, J. R. In *Principles of fluorescence spectroscopy*, 3rd ed.; Springer: New York, 2006; pp 284−286.
(27) Zelent, B.; Kusba, J.; Gryczynski, I.; Johnson, M. L.; Lakowicz, J. R. *J. Phys. Chem.* **1996**, *100*, 18592–18602.
(28) Melo, E.; Martins, J. *Biophys. Chem.* **2006**, *123*, 77–94.

JP103837F